https://doi.org/10.5194/egusphere-2026-6553
Preprint. Discussion started: 9 November 2026
© Author(s) 2026. CC BY 4.0 License.

Satellites and Reanalysis Reveal the Dominance of Dynamics over Precipitation in Marine Cold-Air Outbreak Cloud Break-Up

Filip Severin von der Lippe[1], Tim Carlsen[1], Trude Storelvmo[1], and Robert Oscar David[1]

[1]Department of Geosciences, University of Oslo, Oslo, Norway.

Correspondence: Filip Severin von der Lippe (fslippe@uio.no) and Robert Oscar David (r.o.david@geo.uio.no)

Abstract. Marine cold air outbreaks (CAOs) frequently occur over the North Atlantic during winter, producing characteristic transitions from cloud streets to closed-cell stratocumulus and, eventually, to more broken open cells. The transition to open cells reduces cloud fraction and thus plays an important role in the region's radiative energy balance. However, the drivers of this cloud break-up remain poorly understood.

To investigate these drivers, we apply a newly developed machine learning cloud classifier to MODIS imagery, and combine it with MERRA-2 reanalysis and CloudSat/CALIPSO active remote sensing, enabling a detailed study of CAO cloud fields from the sea ice edge to break-up over the North Atlantic. By identifying break-up as the boundary between closed and open cellular convection, we relate its timing and location to precipitation, cloud phase, marine boundary layer (MBL) structure and instability.

In contrast to earlier studies, we find no direct link between precipitation and break-up. Instead, MBL deepening emerges as the primary control on break-up timing and location. Specifically, break-up is observed only once the MBL deepens to approximately 2 km, a change we associate with reduced cloud-surface coupling, glaciation, and subsequent dissipation of the stratiform cloud layer. We further relate MBL deepening to inversion strength and instability, with weaker inversions and stronger instabilities promoting rapid deepening and break-up. This in turn controls the dominant cloud regime of CAOs, and thereby their radiative impact.

1 Introduction

Marine cold air outbreaks (CAOs) occur when cold, dry air flows from ice- or snow-covered surfaces over a relatively warm ocean. The resulting strong air–sea temperature contrast creates an unstable marine boundary layer (MBL), with intense turbulent heat fluxes (Papritz et al., 2015) that promote rapid cloud formation. Close to the sea ice edge, clouds typically organize as roll convection called cloud streets (Brümmer, 1999; Geerts et al., 2022). These are organized in long bands of shallow clouds aligned with the low-level wind. As the air mass moves farther over the open ocean and the MBL deepens and moistens, these cloud streets often develop into a denser deck of closed-cell stratocumulus clouds, which can eventually break up into more open-cell fields of cumulus and deeper convective clouds (see example Fig. 1A).

Because CAOs are frequent over the Nordic Seas and North Atlantic in winter and spring (Fletcher et al., 2016; Dahlke et al., 2022; von der Lippe et al., 2026), their clouds have a substantial influence on the regional radiative energy balance.

https://doi.org/10.5194/egusphere-2026-6553
Preprint. Discussion started: 9 November 2026
© Author(s) 2026. CC BY 4.0 License.



von der Lippe et al. (2026) estimated that roughly 20 % of the cloud cover in the North Atlantic from December to March is associated with CAOs, implying that any changes in the prevalence or distribution of CAO cloud types in a future climate could significantly alter the surface energy budget. This sensitivity is tied not only to the frequency of CAOs, but also to the evolution of cloud regimes within the CAOs. In particular, the transition from closed cells to more broken open cells is accompanied by a large reduction in cloud fraction and albedo (McCoy et al., 2017), and has therefore been a focus of previous studies investigating cloud evolution and break-up (e.g. Abel et al., 2017; Yamaguchi et al., 2017; Tornow et al., 2021; Murray-Watson et al., 2023).

Despite this interest, the mechanisms controlling the timing and location of break-up within CAOs remain poorly understood. Earlier work has typically either related cloud evolution to distance or time since the air mass left the sea ice edge (e.g. Murray-Watson and Gryspeerdt, 2024; Larsgård et al., 2026), or has been limited to individual CAO case studies (e.g. Abel et al., 2017). As a result, we lack generalizable, statistical predictors of where along a CAO trajectory the stratocumulus deck will break up into open cells.

To address this knowledge gap, we formulate three hypotheses based on previous literature. We examine whether cloud breakup is primarily driven by precipitation (H1), flux-driven deepening and decoupling of the MBL (H2), or instability and turbulence generation (H3):

H1: Precipitation is the main driver of break-up Earlier studies have reported high precipitation rates just before the transition from closed to open cells, suggesting precipitation as a necessity for cloud break-up in CAOs (Abel et al., 2017; Lloyd et al., 2018; Karalis et al., 2022). Through cloud water removal and evaporative (or sublimative) cooling of the sub-cloud layer, precipitation both dries the stratocumulus clouds and creates cold pools that could reorganize the updrafts into open cellular convection (Torri et al., 2015; Saggiorato et al., 2020). The resulting sub-cloud cooling can also sufficiently stratify the MBL to decouple the cloud layer from the moisture supplying surface, so that the stratiform cloud layer slowly dissipates through continuous precipitation and entrainment.

During precipitation, aerosols are scavenged, reducing cloud droplet number concentration N_d. This may further enhance precipitation efficiency and break-up in warmer clouds (Yamaguchi et al., 2017; Goren et al., 2019; Mayer et al., 2026). In the colder clouds examined in this study, the observed reduction in N_d across transitions (Abel et al., 2017) may not necessarily increase precipitation efficiency, but it does confirm the presence of precipitation during break-up. Strong ice formation, which is tightly linked to precipitation (Tornow et al., 2021), has also been observed as the clouds transition from mixed-phase closed cells to more heavily glaciated open cells (Abel et al., 2017; Lloyd et al., 2018). In the Arctic and during CAOs, air masses are relatively clean (Mauritsen et al., 2011), implying low concentrations of ice-nucleating particles (INPs) (Geerts et al., 2022; Gjelsvik et al., 2025) and an important role of secondary ice production (SIP) in enhancing precipitation (Karalis et al., 2022; Pasquier et al., 2022). As SIP is highly temperature dependent (e.g. the Hallett–Mossop mechanism and droplet freezing and fragmentation Hallett and Mossop, 1974; Korolev and Leisner, 2020), break-up may also be temperature dependent, with more efficient break-up occurring in regimes favorable for SIP.

H2: Flux-driven MBL deepening and decoupling is the main driver of break-up
As strong heat fluxes during CAOs rapidly deepen the MBL, conditions evolve downwind from favoring cloud streets to closed-

https://doi.org/10.5194/egusphere-2026-6553
Preprint. Discussion started: 9 November 2026
© Author(s) 2026. CC BY 4.0 License.

cellular and, ultimately, open-cellular convection (Brümmer, 1999). Consequently, factors that control the MBL deepening should also influence how quickly the CAO cloud field breaks up into open cells. Tornow et al. (2023) showed that subsidence delayed deepening and the transition from closed to open cells. Additionally, McCoy et al. (2017) showed that instability as described by the MCAO index (M, Kolstad and Bracegirdle, 2008), was correlated with the frequency of open cell formation, while the estimated inversion strength (EIS, Wood and Bretherton, 2006) showed a negative correlation. This aligns with other research showing that higher M generally leads to a faster reduction in cloud fraction of CAOs (Murray-Watson et al., 2023). We therefore expect cloud breakup to be influenced by processes that deepen the MBL, such as instability, as well as by processes that suppress its deepening, such as subsidence and EIS.

H3: Instability and turbulence generation is the main driver of break-up

A third hypothesis focuses more directly on instability and turbulence generation as controls on cloud regime. Higher instability may itself favor open cellular convection. Thus, a threshold or range of M values might be required for open cellular convection to initiate. As M is related to the air-sea surface contrast and surface fluxes, this idea is consistent with studies of stratocumulus-to-cumulus transitions in the subtropics, where break-up typically occurs as sea surface temperatures increase (Sandu and Stevens, 2011). Additionally, other studies have more frequently observed cellular convection for higher values of the stability parameter $-H/L$ (Klingebiel et al., 2025, 2026; Etling and Brown, 1993), indicating that break-up might not only depend on MBL height (H) itself, but also the relative contribution of wind shear and buoyancy to turbulence generation as indicated by the Monin-Obukhov length (L) (Obukhov, 1946; Monin and Obukhov, 1954).

In total, these three hypotheses suggest that multiple factors such as precipitation processes, surface fluxes, MBL deepening, and the balance between buoyancy and shear-driven turbulence may be controlling the timing and location of break-up in CAO clouds. To investigate these hypotheses, we developed a statistical approach that studies clouds in relation to the observed break-up location, as identified by a CAO cloud classifier applied to satellite imagery. Using this framework, we track 11 years of North Atlantic CAO cloud fields from the sea-ice edge to break-up and open-cell formation, and investigate potential drivers of break-up using MERRA-2 reanalysis (Global Modeling and Assimilation Office (GMAO), 2015), as well as CloudSat radar (Stephens et al., 2002) and CALIPSO lidar (Winker et al., 2009) satellite remote sensing products. Section 2 presents our methods, including an introduction to the cloud classifier. In Section 3, we present our results by addressing each hypothesis individually, before summarizing our work in Section 4.

2 Methods

2.1 Data and model development

Building on our previous work (von der Lippe et al., 2026), we utilize swaths of MODIS thermal infrared images to detect and classify CAO clouds. Specifically, we utilize 1 km MODIS calibrated radiances (band 31, 10.780 - 11.280 μm) from an extended winter period spanning September to May from 2006 to 2017. Using these images, we apply the evaluation methods of von der Lippe et al. (2026) to generate a training dataset for a supervised convolutional neural network (CNN). By looking through images representing both CAO and non-CAO conditions, a human labeler was asked to identify three classes: closed

https://doi.org/10.5194/egusphere-2026-6553
Preprint. Discussion started: 9 November 2026
© Author(s) 2026. CC BY 4.0 License.

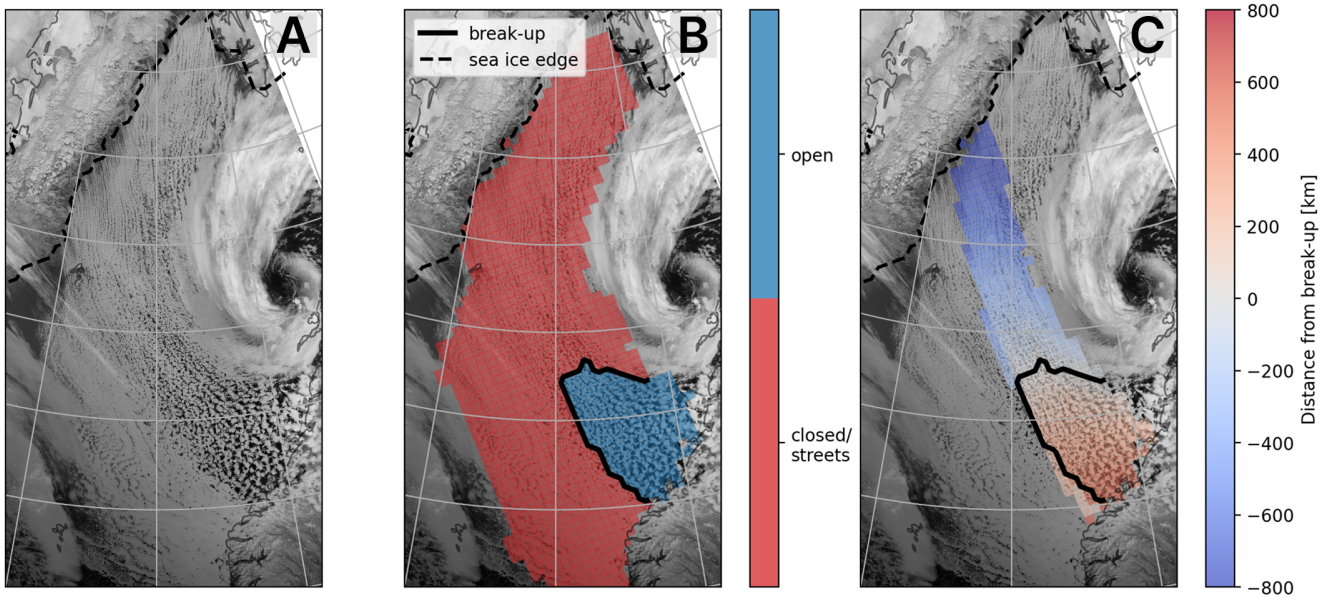


Figure 1. An example classified satellite image from MODIS Terra, 3 March 2023, 20:45 UTC. Panel A shows the MODIS band 31 satellite image of a CAO originating from the Fram Strait in the North, traveling towards Norway in the South-East. Panel B shows the classified image, with break-up being defined as the boundary between closed and open cells. In panel C, the upwind (negative, blue) and downwind (positive, red) distances from the break-up are shown using wind stepping from the defined break-up.

cells (including cloud streets), open cells, and neither, resulting in 500 hand-labeled images. From these labeled images, smaller patches of size 128x128 km were extracted with a stride of 64. This provided patches at a spatial resolution of 64 km, each with a corresponding labeled class. In total, 170,835 patches were extracted and split into 80-20% train-test subsets for training.

The CNN architecture is adapted from the unsupervised model in von der Lippe et al. (2026), utilizing their encoder which has shown great potential in feature extraction of CAO clouds. The encoder compresses image patches through progressively smaller representations to produce a final feature map. This feature map is then processed through a two-layer fully connected neural network to generate a classification. Specifically, the CNN provides probabilities of each input patch belonging to the three predefined classes. The final classification is then defined based on the most probable class, except in situations where the probability of CAO clouds (closed and open combined) exceeds 50%. In these special cases, the final class is the most probable of closed and open.

After training, the model achieved a final test accuracy of 87.2% (See Appendix A), resulting in a classifier that effectively separates closed and open cell regimes, as visualized in Fig. 1B.

https://doi.org/10.5194/egusphere-2026-6553
Preprint. Discussion started: 9 November 2026
© Author(s) 2026. CC BY 4.0 License.

2.2 Calculating distance from break-up

After training the supervised CNN, we applied it to 42,074 MODIS Aqua images to be collocated with CloudSat and CALIPSO from the time period September to May between 2006 and 2017. This time frame was chosen to balance data volume with data quality from CloudSat/CALIPSO. Although CloudSat operated in daytime-only mode after 2011 following a battery failure, the additional 6 years of daytime-only data remain valuable for our statistical analysis until the CALIPSO laser began to degrade in Summer 2017 (Stephens et al., 2018).

Following classification, cloud break-ups were identified as boundaries between closed and open cell regimes. To ensure that these break-ups were closed-to-open cell transitions, we utilized the Modern-Era Retrospective analysis for Research and Applications, Version 2 (MERRA-2, Gelaro et al., 2017) 10-meter wind field to only consider break-ups with closed cells upwind and open cells downwind. Out of the total 42,074 classified images, 12,801 contained a break-up. Given the classification model's spatial resolution of 64 km, these images yielded a total of 112,035 break-up locations.

From every break-up location we utilized the MERRA-2 wind field at the time of the MODIS overpass to create wind transects by stepping both upwind and downwind, 25 km at a time (see Fig. 1C). While not a Lagrangian approach, these transects were considered sufficient to study cloud development, given the consistent wind flow in CAOs (see Appendix B). For each transect we kept track of the CNN-classified cloud class when available, and defined a distance to both break-up and sea ice edge for every wind step point. Here the distance to the sea ice edge is defined as the distance to the first upwind wind-stepping point hitting a sea ice concentration of 0.2 or land such as Svalbard, Novaya Zemlya or Greenland, following the sea ice concentrations from Nimbus-7 SMMR and DMSP SSM/I-SSMIS Passive Microwave Data, Version 2 (DiGirolamo et al., 2022).

By combining distances from both the sea ice edge and break-up, we were able to distinguish CAOs based on their fetch (distance from ice) at break-up. This allowed us to investigate the drivers behind break-up occurring at widely different distances from the ice edge. While this approach provided a powerful framework for studying CAOs, we aimed to also simplify some of our analysis by categorizing CAOs into four classes based on their fetch at break-up: **early** (100–275 km), **early-mid** (275-450 km), **mid-late** (450–625 km), and **late** (625–800 km) break-ups. These category ranges were chosen because we had insufficient closed-cell observations for break-ups occurring closer than 100 km or farther than 800 km from the ice edge.

All CAO-related information described above was then colocated with remote sensing cloud products and reanalysis data. As CloudSat, CALIPSO and the Aqua satellite were all part of the A-train satellite constellation 2006-2017, a close-to-perfect temporal colocation between the cloud classifications and active remote sensing measurements was achieved. After the spatial colocation, we identified a total of 69,676 transects that had at least one wind trajectory point located within 12.5 km of a CloudSat/CALIPSO overpass.

2.3 Remote sensing and reanalysis products

While we require all retrievals to be from areas classified as closed or open cells, the 64 km resolution of our classifications allows for the inclusion of clear sky or non-CAO clouds, even when the larger cloud field consists predominantly of CAO

https://doi.org/10.5194/egusphere-2026-6553
Preprint. Discussion started: 9 November 2026
© Author(s) 2026. CC BY 4.0 License.

clouds. To reduce the influence of non-CAO clouds, we use the 2B-CLDCLASS-LIDAR product (Sassen et al., 2008), which combines retrievals from the CloudSat cloud profiling radar (CPR) and CALIPSO lidar (CALIOP) to define in-cloud CAO conditions. Specifically, we define in-cloud conditions as having a single layer liquid, mixed or ice phase cloud with a cloud phase retrieval confidence of 7/10 or greater. Additionally, we require a cloud top height (CTH) between 30 m and 4000 m. While this restriction may limit retrievals of deeper open cells, we expect such cells to develop primarily after break-up, which is not the focus of this study.

From the phase retrieval, cloud phase fractions are calculated as the ratio of liquid, mixed, or ice-phase clouds to the total number of clouds. In addition, we combine CTH with air temperatures from the ECMWF-AUX product to estimate cloud top temperatures (CTTs). To calculate precipitation fractions, we utilized the precipitation flag from the 2C-PRECIP-COLUMN product (Haynes et al., 2009), while for surface precipitation estimates we relied on the 2C-SNOW-PROFILE product (Wood et al., 2013, 2014). The latter provides estimates of surface snowfall rates based on CloudSat CPR data. Although it only accounts for snowfall, we expect the contribution of rain and drizzle to be minimal at break-up locations within our study time frame and domain.

We also used the CloudSat/CALIPSO-colocated ECMWF-AUX reanalysis product to investigate the potential role of dynamics and instability on cloud break-up. In particular, we focused on atmospheric instability as indicated by the commonly used M-index:

$$M = \theta_s - \theta_{850}, \tag{1}$$

calculated as the potential temperature difference between air at 850 hPa (θ_{850}) and the sea surface (θ_s). We also investigated the role of the inversion strength by calculating the EIS:

$$\mathrm{EIS} = \mathrm{LTS} - \Gamma_m^{850}(z_{700} - z_{\mathrm{LCL}}). \tag{2}$$

Here we have the height of 700 hPa and the lifting condensation layer (LCL) denoted as z_{700} and z_{LCL} respectively, and the lower troposphere stability LTS as:

$$\mathrm{LTS} = \theta_{700} - \theta_0. \tag{3}$$

Finally, the moist-adiabatic potential temperature gradient is calculated as:

$$\Gamma_m = \frac{g}{c_p}\left(1 - \frac{1 + L_v q_s/(R_d T_{850})}{1 + L_v^2 q_s/(c_p R_v T_{850}^2)}\right), \tag{4}$$

where g is the gravitational acceleration, c_p is the specific heat of air at constant pressure, L_v is the latent heat of vaporization, q_s is the saturation mixing ratio at the temperature of the 850 hPa level (T_{850}), and R_d and R_v are the gas constants for dry and moist air, respectively.

Since the LCL is not provided by the ECMWF-AUX product, we use the retrieved CBH from the 2B-CLDCLASS-LIDAR product as an estimate.

https://doi.org/10.5194/egusphere-2026-6553
Preprint. Discussion started: 9 November 2026
© Author(s) 2026. CC BY 4.0 License.

To estimate the stability parameter -H/L, we used the CTH from the 2B-CLDCLASS-LIDAR product as a proxy for the MBL height (H). The Monin-Obukhov stability length was calculated similar to Brümmer (1999) as:

$$L = -\frac{\overline{\theta}}{gk}\frac{(c_D U_{10}^2)^{2/3}}{c_H \Delta\theta_{as} U_{10}}. \tag{5}$$

where, U_{10} is the 10 m wind speed, $k = 0.4$ is the von Kármán constant, and the momentum and heat flux transfer coefficients were assumed to be equal at $c_D = c_H = 1.3 \times 10^{-3}$. Finally, the mean potential temperature was calculated using the ECMWF-AUX 2 m and 0 m potential temperatures $\overline{\theta} = \frac{\theta_0 + \theta_2}{2}$, and the air-sea temperature difference was calculated as $\theta_{as} = \theta_2 - \theta_{sst}$.

By combining reanalysis and active remote sensing products with neural network-derived information about break-up locations and the ice edge, we compiled a database of measurements binned within a two-dimensional space defined by 25 km by 25 km intervals of distance from both break-up and ice edge. This approach allowed us to distinguish CAOs according to their fetch at break-up, helping to better understand the widely varying cloud developments within CAOs.

3 Results and discussions

In this section, we evaluate the three hypotheses introduced above. First, we test whether precipitation occurrence and intensity are consistently related to the timing and location of cloud break-up (H1). Second, we examine whether MBL depth, deepening rate, inversion strength, instability, and subsidence support flux-driven MBL deepening and decoupling as the main control on cloud break-up (H2). Third, we assess whether instability and the relative roles of buoyancy and shear in generating turbulence more directly drive the transition to open-cell convection (H3). Finally, we combine the results to develop a conceptual picture of cloud break-up in CAOs.

3.1 H1: Precipitation is the main driver of break-up

3.1.1 Median precipitation rates

To investigate the role of precipitation in driving break-up, we first observe the fraction of precipitating in-cloud observations in Fig. 2A. Here we see that close to 100 % of our closed cell observations are precipitating once the clouds have traveled around 75 km from the ice edge. While the constant precipitation suggests that break-up is independent of the precipitation onset, we also need to investigate precipitation rates as observed in Fig. 2B. This figure shows generally low median precipitation rates (<0.06 mm/hr), consistent with light snowfall found in previous studies (Mateling et al., 2023). We also find the highest median precipitation rates at 100-250 km from the ice edge, rather than at or just before break-up. This phenomenon is further discussed in Appendix C, and suggests that median precipitation rates alone are unable to explain the timing and location of break-up.

However, surface precipitation is derived from the lowest bin above the CPR clutter zone (Wood and L'Ecuyer, 2018), which introduces uncertainties into the retrievals. While the median surface precipitation rates may be inaccurate, it is unlikely that the highest precipitation retrievals would consistently occur outside break-up regions if precipitation was the main driver.

https://doi.org/10.5194/egusphere-2026-6553
Preprint. Discussion started: 9 November 2026
© Author(s) 2026. CC BY 4.0 License.

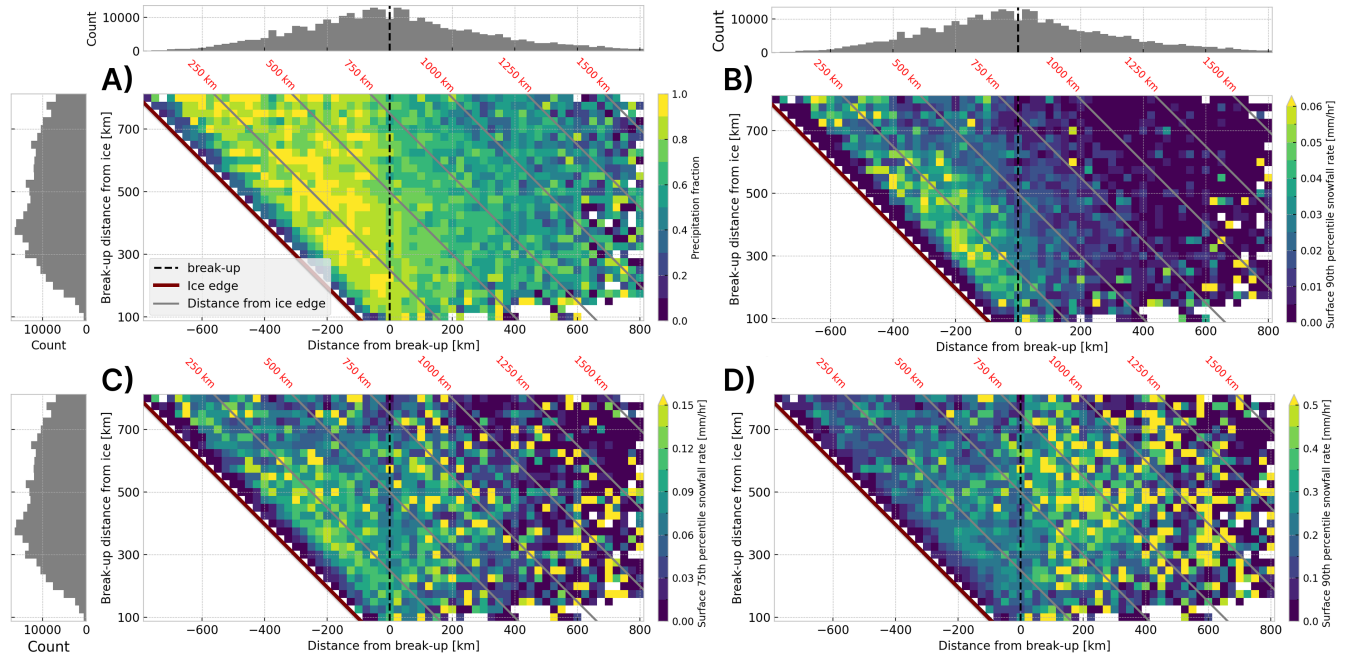


Figure 2. Precipitation as a function of distance to break-up, distance from the ice edge, and break-up distance from the ice edge. Each row of bins corresponds to CAOs with break-ups occurring at a specific distance from the ice edge, while each column corresponds to a given distance from the break-up. Combining these two dimensions, a measure of distance from the ice edge is represented along the diagonal axis, with distances indicated in red. The cumulative counts for each distance-from-break-up and break-up-distance-from-ice bin are shown above and to the left of the panels, respectively. Panel A shows the precipitation fraction retrieved from the 2C-PRECIP-COLUMN product, while Panels B, C, and D show the median, 70th percentile, and 90th percentile surface snowfall rates from the 2C-SNOW-PROFILE product.

Furthermore, previous studies have demonstrated CloudSat's high sensitivity to light snowfall (Cao et al., 2014), reinforcing our conclusion that median precipitation rates are insufficient to explain cloud break-up.

3.1.2 Precipitation maxima

The median precipitation rates observed in Fig. 2B give a good overview of the general precipitation pattern, but fail to detect the distribution of precipitation and outliers that could help to initiate cloud break-up. We therefore investigate if some embedded higher precipitation rates are all it takes to initiate break-up across the closed cell cloud layer. This idea is consistent with observations of CAO clouds, where precipitation rates of up to 3 mm/hr have been observed to develop cold pools (Ephraim et al., 2026). To further investigate this, we present in Fig. 2C and D, the 75th and 90th percentile precipitation rates. While we do observe some higher 90th percentile precipitation rates after break-up, the rates are still relatively low and are expected due to the more convective nature of the open cells. These enhanced rates could however maintain the open cellular convection through cold pool creation, but as they are observed after break-up, the enhanced rates are not seen as drivers of break-up.

https://doi.org/10.5194/egusphere-2026-6553
Preprint. Discussion started: 9 November 2026
© Author(s) 2026. CC BY 4.0 License.

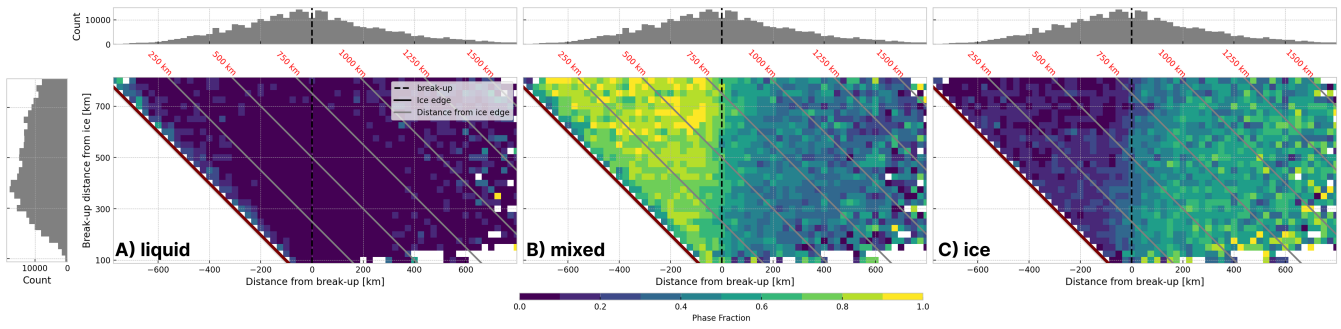


Figure 3. Median cloud phase fraction as a function of distance to break-up, distance from the ice edge, and break-up distance from the ice edge (same as Fig. 2). Cloud phase fractions are retrieved from the 2B-CLDCLASS-LIDAR product.

In the 70th percentile in panel C, the same pattern as for the median in panel B emerges, where a band of higher precipitation rates is found closer to the ice edge instead of immediately before break-up. Consequently, neither the 70th or 90th percentiles suggest precipitation rates that are sufficiently different before or at break-up for H1 to be confirmed.

3.1.3 Cloud phase

While no clear signal in precipitation rates is found, earlier studies have suggested cloud glaciation as an important contributor to both precipitation and break-up (Abel et al., 2017). To investigate the role of glaciation, we analyze the cloud phase as observed in Fig. 3. This figure shows the median liquid (A), mixed (B) and ice (C) phase fractions as a function of distance from break-up and break-up distance from ice. First, in panel A we notice that liquid-only clouds are relatively rare (below 10 %) in both the closed and open cell regime, with slightly higher liquid phase fractions occurring just off the sea ice edge (up to 60 %). This aligns with the findings of previous research (Carlsen and David, 2022; Murray-Watson and Gryspeerdt, 2024), that have proposed that lacking INPs over sea ice result in higher concentrations of supercooled liquid clouds. As these clouds traverse the open ocean, marine organic INP sources may become available, which results in a declining fraction of liquid-only clouds. This becomes evident when considered together with panel B, which shows an increase in mixed-phase cloud fractions at the expense of liquid-only clouds. The fraction of mixed-phase clouds then generally stays above 70 % until break-up, where a rapid decline in the mixed-phase fraction to around 40 % is observed. Panel C further shows that this decline is clearly attributable to increased glaciation, apparent from the increasing fraction of ice clouds after break-up.

This pattern is further detailed in Fig. E1, which illustrates the variability in the observed phase fractions. Here, the median mixed-phase and ice-phase fractions approach 30 % and 60 %, respectively, in the open-cell regime. The phase signal also partially aligns with the cloud top temperatures (CTTs) shown in Fig. F1 panel A. Specifically, we observe median CTTs above -15°C for break-ups occurring farther than 600 km from the ice edge while they generally stay below -20°C for earlier break-ups. This could help explain the delayed glaciation signal through slower ice production in these CAOs. Additionally, the liquid water path (LWP) and ice water path (IWP) patterns in Fig. F1B and C are consistent with the CTT signal, increasing our

https://doi.org/10.5194/egusphere-2026-6553
Preprint. Discussion started: 9 November 2026
© Author(s) 2026. CC BY 4.0 License.

confidence that CTT plays a role in modulating ice production. However, as CTTs do not align as clearly for earlier break-ups, we remain unable to generalize the influence of CTT on the observed glaciation signal.

Taken together, the precipitation results do not support H1: precipitation is not the universal driver of CAO cloud break-up. Precipitation is already nearly ubiquitous throughout much of the closed-cell regime, and neither median nor upper-percentile snowfall rates show a systematic maximum at or immediately before break-up. Instead, the highest typical precipitation rates occur at a characteristic distance of approximately 100–250 km from the ice edge, largely independent of the fetch at which break-up occurs. Precipitation intensity therefore does not explain why otherwise similar CAOs break up at widely different fetches.

The pronounced transition from mixed-phase to glaciated clouds at break-up shows that microphysical changes accompany the transition. However, because no corresponding precipitation-rate increase is observed at break-up, our data do not support glaciation and following precipitation as the direct trigger of cloud break-up. Precipitation may nevertheless contribute indirectly by removing cloud water and through sublimation-driven cooling below cloud base, which could promote stratification and cloud–surface decoupling. Thus, we cannot exclude precipitation as a contributing process or as a driver in particular CAO cases, but reject precipitation intensity as a general predictor and primary trigger of break-up across the sampled CAOs.

3.2 H2: Flux-driven MBL deepening and decoupling is the main driver of break-up

To investigate the role of the MBL depth on the timing and location of break-up, we use the retrieved CTH from 2B-CLDCLASS-LIDAR as a proxy for the MBL depth. Although CTH is not a perfect proxy, we expect cloud-top height to closely track MBL deepening due to the strong surface fluxes during CAOs. The evolution of the median CTH is shown in Fig. 4A, as well as separated into classes of early, early-mid, mid-late and late break-ups in panels B-E, respectively. Here we observe a typical CTH of approximately 2 km at the identified break-ups, with half of the observations falling in the CTH range of 1690-2230 m. While this indicates that there is no critical CTH at which break-up occurs, it suggests that a sufficiently deep MBL is a necessary precondition for break-up.

As CTH at break-up is relatively consistent for all CAOs, it becomes evident that earlier break-ups are associated with more rapid deepening of the MBL than late break-ups. This is observed in Fig. 4, with MBL deepening rates of 272 m and 113 m per 100 km for early (panel B) and late (panel E) break-ups, respectively. To better understand break-up, we therefore investigate factors such as the EIS and M-index as potential factors controlling the rate of deepening of the MBL.

In Fig 5A, we observe the initial inversion strength of the MBL as indicated by the EIS at 50 km from the ice edge. Here, we choose 50 km and not right at the ice edge to remove the influence of the marginal ice zone, and to make sure the MBL has developed beyond depths at which remote sensing instruments are unable to retrieve. With a moderate Pearson correlation coefficient of 0.43, we observe generally lower initial EIS for earlier break-ups and higher EIS for later break-ups. This is consistent with a strong inversion limiting the rate at which the MBL can deepen. Furthermore, the instability, as indicated by the M-index in Fig. 5B and E, shows the opposite signal with a weak correlation coefficient of -0.21, 50 km from the ice edge and -0.32 at break-up. This shows that higher M-indices are generally found for earlier break-ups, helping to more quickly develop the MBL to CTHs where break-up typically occurs. Additionally, we investigate the role of subsidence in Appendix

https://doi.org/10.5194/egusphere-2026-6553
Preprint. Discussion started: 9 November 2026
© Author(s) 2026. CC BY 4.0 License.

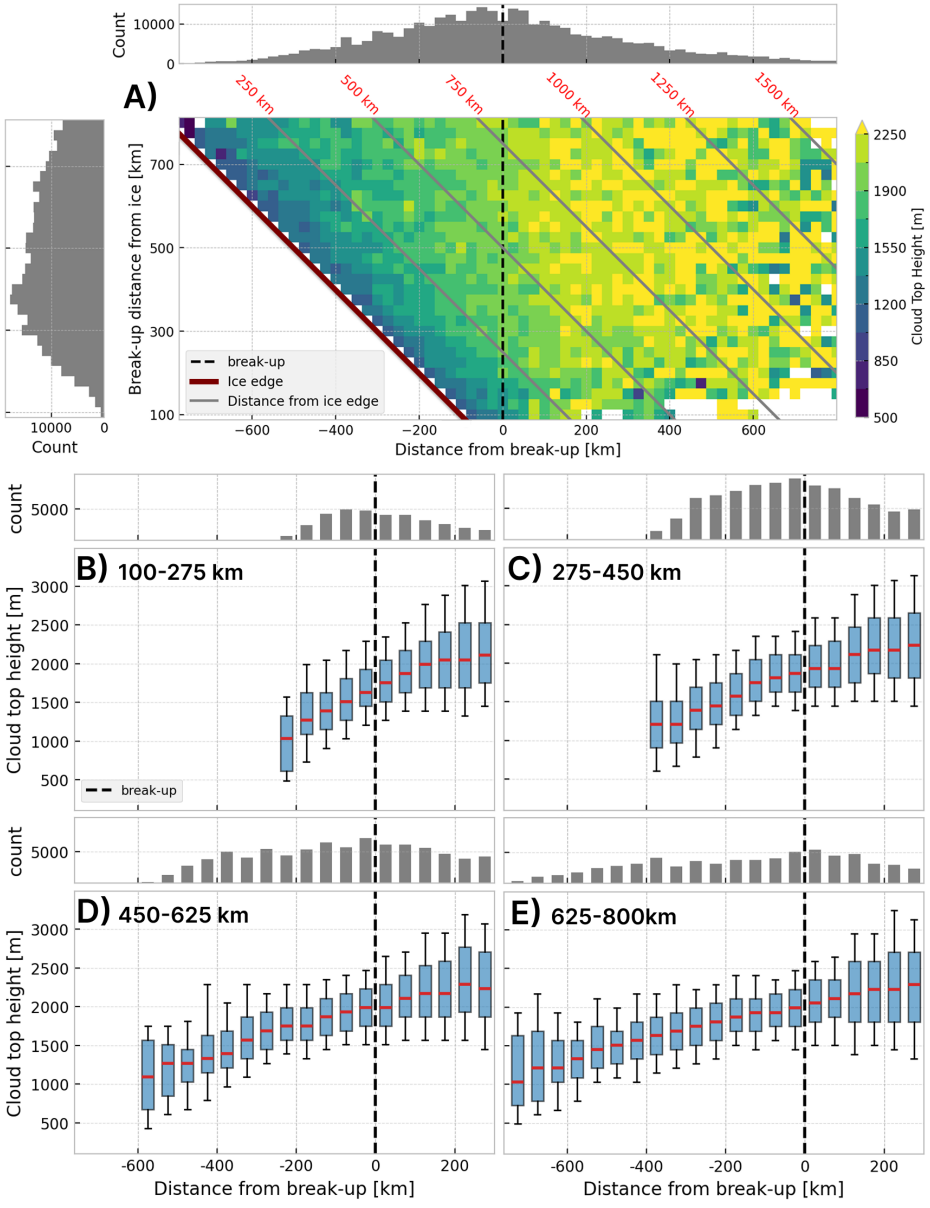


Figure 4. Evolution of the CTH retrieved from the 2B-CLDCLASS-LIDAR product. Panel A shows the median CTH as a function of both distance from break-up and break-up distance from ice, while panels B-E show the CTH evolution for CAOs breaking up at different distance ranges from the sea ice indicated in each panel. Here, red lines indicate the medians, boxes show the 25th–75th percentiles, and whiskers show the 10th–90th percentiles. The MBL deepening rates from the ice edge to break-up are 272, 193, 144 and 113 m per 100 km for panel B (early), C (early-mid), D (mid-late), and E (late) respectively.

https://doi.org/10.5194/egusphere-2026-6553
Preprint. Discussion started: 9 November 2026
© Author(s) 2026. CC BY 4.0 License.

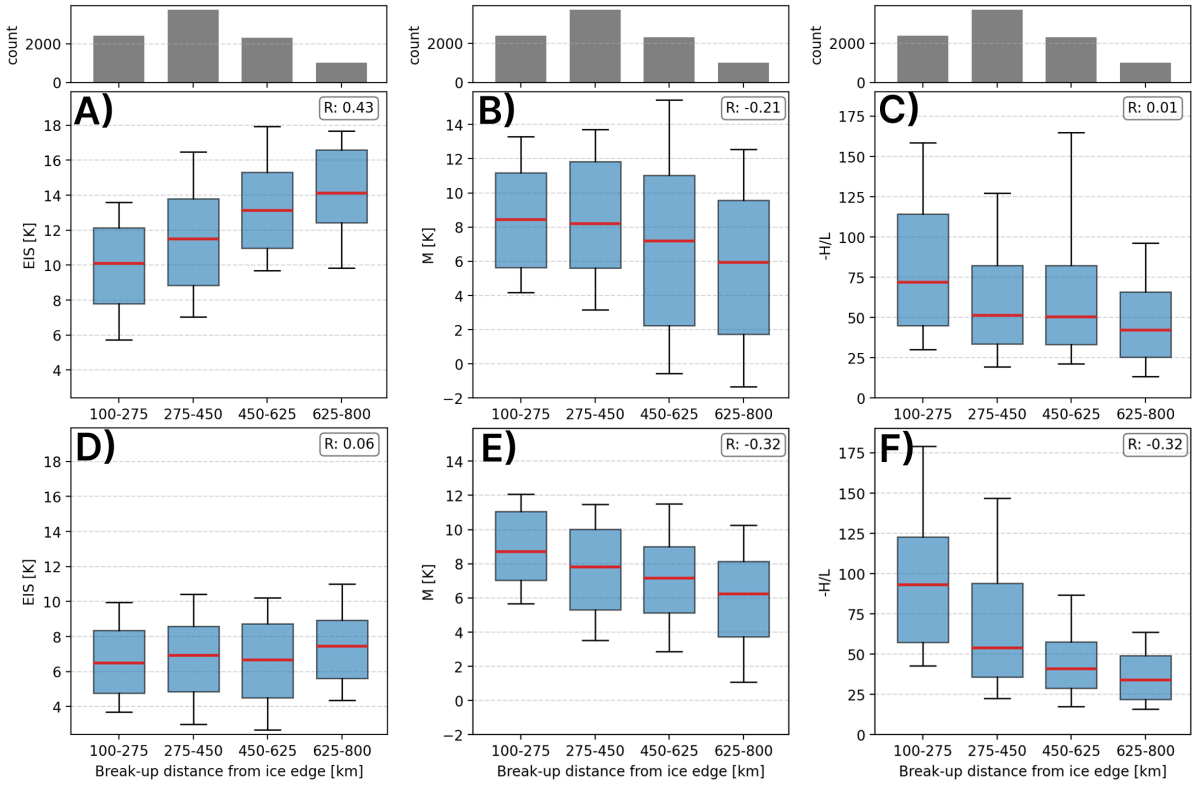


Figure 5. The EIS, M-index and -H/L at 50 km from the ice edge (A-C) and at break-up (D-F) for the same four classes of early, early-mid, mid-late and late break-ups as in Fig. 4. Red lines indicate the medians, boxes show the 25th–75th percentiles, and whiskers show the 10th–90th percentiles.

D, which shows a weak correlation of 0.1 with stronger subsidence being linked to delayed break-up. Although weak, this relationship aligns with the work of Tornow et al. (2023), which linked subsidence with delayed break-up.

Despite the substantial differences in EIS close to the ice edge, EIS values at break-up converge toward a similar range across all break-up-fetch categories (Fig. 5D). This pattern suggests that break-up may be more likely once the inversion has weakened sufficiently. However, the results do not identify a universal EIS threshold for break-up.

Overall, the results support H2 and identify flux-driven MBL deepening as the strongest control on the timing and location of break-up in our analysis. Break-up consistently occurs after the cloud layer has deepened to approximately 2 km, while CAOs that break up closer to the ice edge reach this depth more rapidly than those that break up farther downstream. This faster deepening is associated with weaker initial inversions, greater instability, and weaker subsidence.

These relationships are also evident in Lagrangian back trajectories from the ice edge based on the MERRA-2 reanalysis (Appendix B). In these trajectories, EIS and the M-index show correlation coefficients of 0.32 and -0.25, respectively (Fig. B1), further supporting their roles in controlling CTH and break-up.

https://doi.org/10.5194/egusphere-2026-6553
Preprint. Discussion started: 9 November 2026
© Author(s) 2026. CC BY 4.0 License.

3.3 H3: Instability and turbulence generation is the main driver of break-up

H3 differs from H2 by proposing that instability affects break-up directly through changes in cloud organization, rather than mainly accelerating MBL deepening. Under H3, stronger CAOs, characterized by larger M values, are expected to favor and potentially accelerate the transition to open-cellular convection. In addition, previous studies have found that values of $-H/L$ above 15 favor cellular convection (Etling and Brown, 1993; Klingebiel et al., 2026). Evidence supporting H3 would therefore include a distinct transition threshold in either M or $-H/L$, or a break-up relationship that persists after accounting for MBL depth.

To investigate H3, we first examine the M-index at break-up, as shown in Fig. 5E. Consistent with H3, we observe generally higher M indices for earlier break-ups, with a correlation coefficient of -0.32. However, this relationship alone cannot distinguish between the two proposed pathways. Stronger instability may accelerate break-up indirectly by deepening the MBL, as proposed in H2. Alternatively, it may act directly by promoting a transition from roll to cellular convection, as proposed in H3.

Therefore, we analyze -H/L at both break-up and ice edge as observed in Fig. 5C and F. While no correlation is found at the ice edge, a correlation of -0.32 is found at break-up. Furthermore, earlier break-ups exhibit median stability parameter values approaching 100, indicating conditions highly favorable for cellular convection and potentially explaining their rapid transition to open cells. Later break-ups show median values closer to 25, which still generally favor cellular convection.

These results provide partial support for H3. Although higher values are associated with earlier break-ups, the substantial variability indicates that there is no clear -H/L threshold that triggers the transition. While -H/L may influence the likelihood of transition, it does not alone determine break-up timing. We therefore find no evidence that instability or turbulence generation alone is a sufficient, independent trigger of cloud break-up. Instead, H3 appears to describe a process that can facilitate the transition and modulate its timing, while its strongest influence likely operates through the MBL-deepening pathway described in H2.

3.4 A combined conceptual picture

Our results show a clear phase signal across the transition: the mixed-phase fraction remains high in the closed-cell regime and drops sharply as the clouds glaciate at break-up. This is consistent with earlier studies (Abel et al., 2017; Tornow et al., 2021); however, we cannot directly link the observed glaciation to precipitation or cloud break-up. Instead, we interpret glaciation as a consequence of break-up, occurring only after moisture resupply to the cloud layer has been sufficiently reduced.

With cloud ice consistently growing at the expense of cloud liquid water through the Wegener-Bergeron-Findeisen (WBF) process (Wegener, 1911; Bergeron, 1935; Findeisen, 1938), coupling between the moisture-supplying surface and the cloud layer is required to maintain mixed-phase clouds. To compensate for the loss of liquid water, sustained updrafts transporting moisture-rich air from the surface must be maintained. While the strong surface fluxes of CAOs (Renfrew and Moore, 1999; Papritz and Spengler, 2017) can sustain these updrafts and maintain surface-cloud coupling for a relatively long time, the MBL may eventually become too deep for this coupling to persist. At this stage, updrafts no longer reach cloud base, depleting

https://doi.org/10.5194/egusphere-2026-6553
Preprint. Discussion started: 9 November 2026
© Author(s) 2026. CC BY 4.0 License.

the remaining liquid water. Meanwhile, ice crystals may continue to grow through aggregation and precipitate, ultimately dissipating the remaining cloud.

Within this framework, precipitation is not the trigger for break-up, but it may contribute through sublimation-driven cooling below cloud base, which can increase MBL stratification and weaken cloud-surface coupling. While we cannot confirm this pathway, our results rule out precipitation intensity alone as a universal trigger for cloud break-up in CAOs.

This leaves dynamics related to MBL deepening as the factors with the highest predictive power for break-up. Specifically, the fetch at break-up is moderately correlated with EIS and M just off the ice edge, as well as with M and the stability parameter $-H/L$ at break-up. However, the relatively weak correlations suggest that the pathway to break-up is complex and potentially influenced by additional factors not investigated in this study.

4 Conclusions

Here, we used a newly developed machine-learning cloud classifier applied to MODIS infrared imagery to track CAO cloud fields from the sea-ice edge to break-up over the North Atlantic during 2006–2017. We combined these classifications with CloudSat/CALIPSO cloud products and MERRA-2 reanalysis data, and used a statistical approach to investigate the timing and location of break-up and its relation to precipitation, MBL structure, and instability. By relating atmospheric conditions to the observed break-up location across 11 years of CAOs, our framework extends previous observational and modeling studies that have primarily focused on individual events or cloud evolution as a function of fetch from the ice edge. Using this, we evaluate three hypotheses for cloud break-up drivers: precipitation (H1), MBL deepening and decoupling (H2), and instability and turbulence generation (H3)

Regarding H1, we find that precipitation is already frequent and of similar magnitude throughout the closed-cell regime, with no systematic maximum at or immediately before break-up. This rules out precipitation intensity alone as a universal trigger for break-up in CAOs. Instead, we observe maximum precipitation rates occurring 100–250 km from the ice edge, independent of break-up location. This result challenges the generalizability of observational and model case studies, which suggest that enhanced precipitation immediately preceding the transition is required for break-up (e.g. Abel et al., 2017; Karalis et al., 2022). At the same time, our results do not exclude precipitation as a contributing process in individual events. Specifically, precipitation may act as a continuous cloud-water removal process that contributes to stratification and decoupling through sublimation-driven cooling below cloud base.

Aligning with H2, we find that break-up tends to occur when CTH reaches approximately 2 km. Consequently, we observe that CAOs that break up closer to the ice edge show a faster deepening of the MBL and are associated with weaker initial EIS, weaker subsidence, and larger M. These results extend the findings of McCoy et al. (2017), who linked CAO cloud regime to EIS and M, by directly relating these quantities to the location and timing of break-up. Additionally, it supports the findings of Tornow et al. (2023), which showed that subsidence suppressed MBL deepening and delayed break-up. Together, this identifies flux-driven MBL deepening, modulated by inversion strength, instability, and subsidence, as the strongest statistical control on the timing and location of CAO cloud break-up.

https://doi.org/10.5194/egusphere-2026-6553
Preprint. Discussion started: 9 November 2026
© Author(s) 2026. CC BY 4.0 License.

For H3, earlier break-ups tend to occur under conditions with higher $-H/L$, indicating a larger role for buoyancy-driven turbulence that favors conditions for cellular convection. While this is partly consistent with previous studies (e.g. Etling and Brown, 1993; Klingebiel et al., 2026), we find no universal threshold in either $-H/L$ or M for determining the location and timing of break-up. We instead see instability and turbulence generation as modulators of the timing of break-up.

The strongest and most consistent signal across the transition is a sharp shift in cloud phase. The mixed-phase fraction remains high in the closed-cell regime before rapidly declining as the ice fraction increases at break-up. This glaciation signal is consistent with previous studies (e.g. Abel et al., 2017; Tornow et al., 2021), but we show that it is not accompanied by a universal increase in precipitation intensity. This motivates, but does not directly demonstrate a decoupling-based glaciation interpretation: We propose that glaciation occurs once liquid-water depletion by precipitation and ice growth is no longer balanced by moisture resupply, which is reduced as flux-driven MBL deepening promotes MBL decoupling. However, the exact roles and temporal ordering of these processes remain unresolved by the present satellite and reanalysis data.

Overall, our results suggest that CAO cloud-field evolution and break-up are best understood as an evolving boundary-layer process, rather than as a response to precipitation intensity or onset alone. This shows the need for correctly representing MBL dynamics in weather and climate models to accurately simulate CAO cloud evolution. However, given the sensitivities and uncertainties of satellite retrievals and reanalysis products, future work should test the proposed decoupling pathway using observations and models that resolve the vertical thermodynamic and turbulent structure of the MBL. Aircraft observations, dropsondes, and active remote-sensing observations from EarthCARE (Illingworth et al., 2015; Wehr et al., 2023), together with high-resolution modeling, can help determine the respective roles of cold pools, sub-cloud sublimation, ice-nucleating particles, and secondary ice production in individual CAO transitions. Such work is also needed to determine how future changes in CAO instability, turbulence, and MBL deepening could shift the timing of cloud break-up, with consequences for cloud fraction, albedo, and regional radiative effects of CAOs.

Code and data availability. MODIS level 1B calibrated radiances can be accessed at https://ladsweb.modaps.eosdis.nasa.gov/search/order/1/MOD021KM--61 (MODIS Characterization Support Team (MCST), 2017). NIMBUS sea ice concentration data is available at https://nsidc.org/data/nsidc-0051/versions/2 (DiGirolamo et al., 2022). The MERRA-2 reanalysis products are accessible at https://disc.gsfc.nasa.gov/datasets/M2T1NXSLV_5.12.4/summary (Global Modeling and Assimilation Office (GMAO), 2015). CloudSat/CALIPSO products are available from https://www.cloudsat.cira.colostate.edu/.

Appendix A: Model performance

To evaluate the classification model, we calculated the confusion matrix shown in Fig. A1. This figure shows the fraction of predictions assigned to each class given the true class. Overall, the model performs well as indicated by the high percentages along the diagonal. However, we do observe that the model struggles in classifying closed cells accurately, with 23.9 % of true closed cells being classified as neither. While we do not explore the specific misclassifications in detail, they might partly be a result of discrepancies in the evaluation dataset. Nevertheless, this is not a major concern since the model is more likely

https://doi.org/10.5194/egusphere-2026-6553
Preprint. Discussion started: 9 November 2026
© Author(s) 2026. CC BY 4.0 License.

to avoid making an incorrect labeling of a closed or open cell, than misclassify them. Therefore, we have confidence in the classifications and break-ups identified by the model.

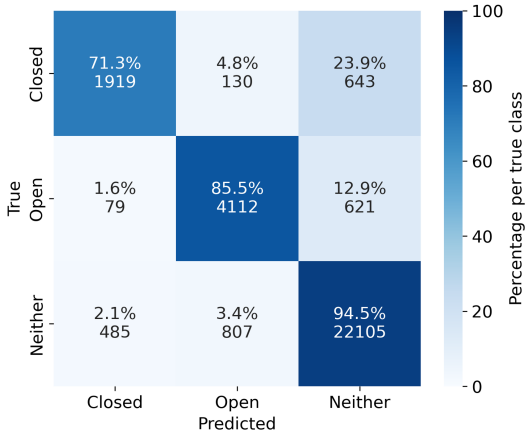


Figure A1. Confusion matrix showing model performance on unseen test data. Percentages indicate the fraction of predictions assigned to each class given the true class. Numbers represent the total predictions made for each true class.

Appendix B: Lagrangian trajectories

Earlier studies have focused on how CAO clouds develop as a function of time since ice (e.g. Murray-Watson and Gryspeerdt, 2024). While this indicates how cloud properties evolve on average as the clouds traverse the ocean, it does not allow us to examine cloud properties relative to break-up. However, with our automatized break-up detection, we can utilize the MERRA-2 wind field to step back in time to investigate the relation between the meteorological background at the sea ice edge and the time and distance to cloud break-up.

Our Lagrangian framework for calculating time to break-up uses the MERRA-2 wind field at the time and location of break-up to step backward in time in 30-minute increments. At each step, we extract the wind field closest in time and space to the updated location and continue stepping backward until reaching a sea ice concentration of 20 %.

While this approach does no longer provide collocated satellite retrievals, it enables us to use reanalysis data to investigate air masses from their departure at the sea ice edge to cloud break-up. This helps us understand why cloud break-up occurs at varying fetches.

https://doi.org/10.5194/egusphere-2026-6553
Preprint. Discussion started: 9 November 2026
© Author(s) 2026. CC BY 4.0 License.

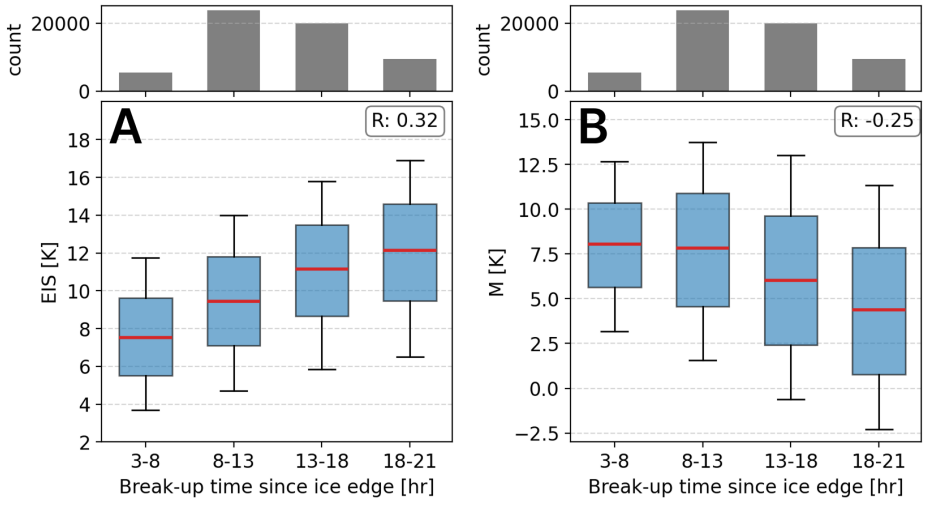


Figure B1. Similar to Fig. 5, but with break-up time since ice instead of fetch. The EIS and M index are calculated using MERRA-2 reanalysis, 1.5 hours from the ice edge. Red lines indicate the medians, boxes show the 25th–75th percentiles, and whiskers show the 10th–90th percentiles.

Similar to Fig. 5, Fig. B1 shows the EIS and M index following air-mass departure from the ice edge. To ensure comparability with the non-Lagrangian analysis, we evaluated these stability parameters at 1.5 hours since the ice edge, corresponding to approximately 50 km from the ice edge in Fig. 5, based on typical wind speeds of about 10 m/s. Using this approach, we observe slightly lower correlations for EIS and higher correlations for the M index. However, the overall message remains consistent: greater instability, indicated by higher M, is associated with earlier break-up, whereas higher EIS corresponds to later break-up. This supports our conclusion that EIS and M govern the deepening rate of the MBL and, consequently, the timing of cloud break-up.

These results also suggest that our non-Lagrangian approach captures the general development of CAOs. This is further confirmed in Fig. B2, where non-Lagrangian trajectories closely align with Lagrangian distances and times since ice, demonstrating the stability of wind fields during CAOs.

https://doi.org/10.5194/egusphere-2026-6553
Preprint. Discussion started: 9 November 2026
© Author(s) 2026. CC BY 4.0 License.

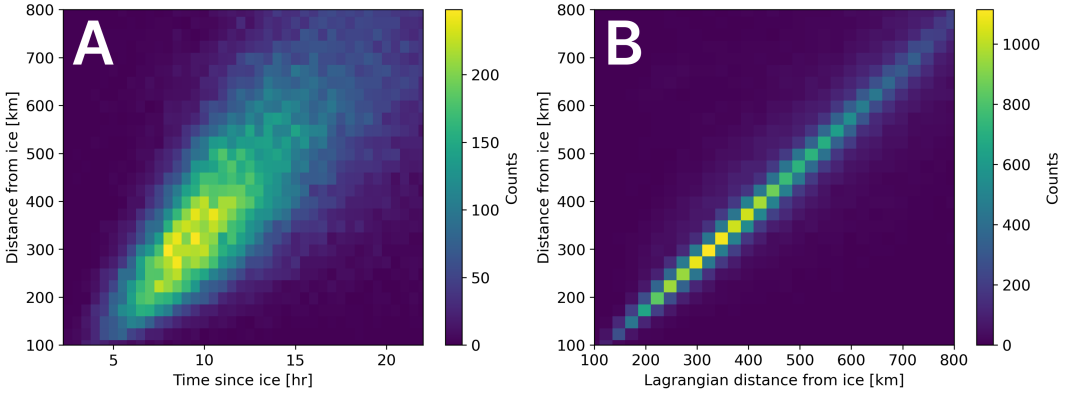


Figure B2. Histograms of the relationship between Lagrangian and non-Lagrangian trajectories. Panel A shows non-Lagrangian distance from ice versus Lagrangian time since ice, while panel B shows non-Lagrangian versus Lagrangian trajectory distance from ice.

Appendix C: Precipitation as function of distance from ice

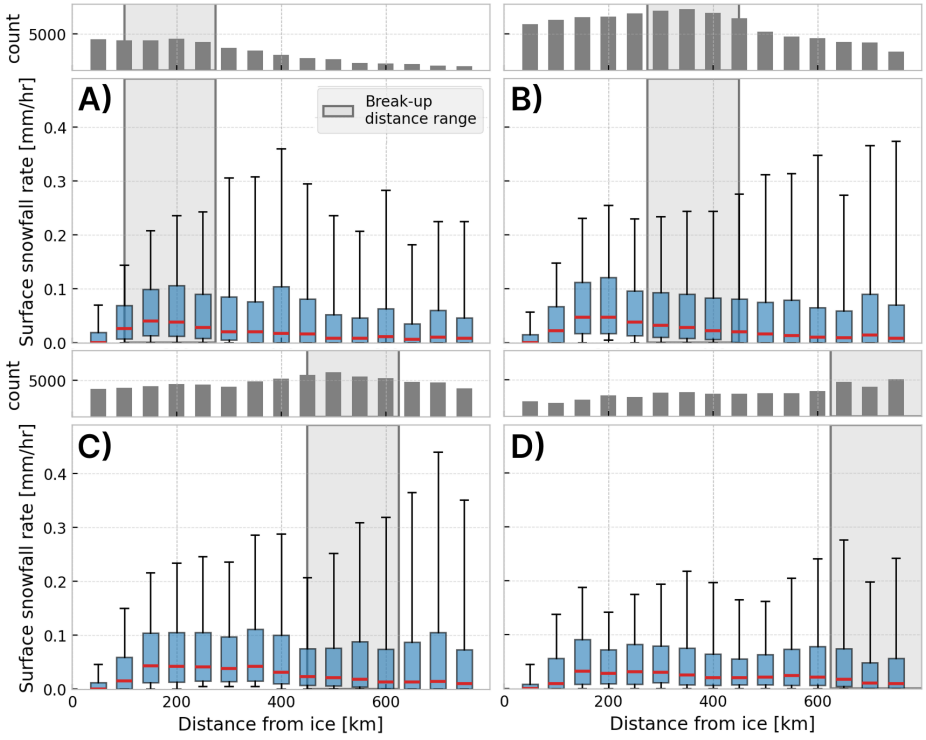


Figure C1. Boxplots showing the surface snowfall rate in mm/hr at 50 km distance bins from the ice edge. The red lines indicate the median, the boxes the 25-75th percentiles, and the whiskers the 10-90th percentiles. The different panels show transects where break-up occurred at different fetch ranges. These were 100-275, 275-450, 450-625, and 625-800 km from ice for panels A), B), C) and D) respectively.

https://doi.org/10.5194/egusphere-2026-6553
Preprint. Discussion started: 9 November 2026
© Author(s) 2026. CC BY 4.0 License.

To investigate the precipitation pattern closer to the ice edge, we show precipitation rates as a function of distance from ice in Fig. C1 for the break-up categories, early, early-mid, mid-late, and late in panels A-D respectively. Here it becomes clear that the location of the generally highest precipitation rates are independent of fetch at break-up, but occur at characteristic distances from the ice edge. In all four panels we observe the highest median precipitation rates at 100-250 km from the ice edge. Again, we generally observe enhanced precipitation maxima after break-up, but as these maxima occur after break-up, we remain unable to use precipitation as a predictor for the timing and location of break-up.

Appendix D: The role of subsidence

To investigate the role of subsidence on the timing of break-up, we use the omega parameter at 700 hPa from MERRA-2 reanalysis, as shown in Fig. D1. This figure indicates that CAOs with later break-ups experience stronger subsidence compared to earlier break-ups. To further investigate its potential influence on delaying break-up, we calculate ice-to-break-up trajectory means of omega and correlate them with fetch at break-up. This yields a weak correlation coefficient of 0.1, suggesting a minimal influence of subsidence break-up timing. These findings relate back to H2, where stronger subsidence may limit the deepening rate of the MBL and thus delay break-up, such as observed by Tornow et al. (2023).

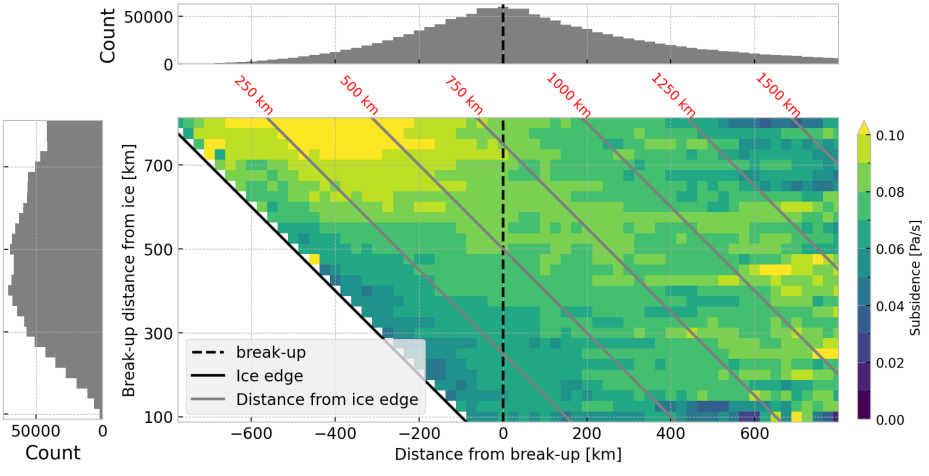


Figure D1. Subsidence at 700 hPa from MERRA-2 reanalysis for the same distance bins as described in Fig. 2.

Appendix E: Cloud phase

In addition to the two-dimensional cloud phase development shown in Fig. 3, we investigate phase fractions as a function of distance from break-up in Fig. E1. This figure more clearly captures the glaciation signal across the transition, with the median mixed-phase fraction decreasing from above 90 % to below 40 % as clouds transition into the open-cell regime. However, the phase fractions vary considerably across different CAO events, as indicated by the boxes and whiskers, suggesting that

https://doi.org/10.5194/egusphere-2026-6553
Preprint. Discussion started: 9 November 2026
© Author(s) 2026. CC BY 4.0 License.

glaciation of individual clouds can occur well within the closed-cell regime without necessarily leading to break-up across the entire cloud field.

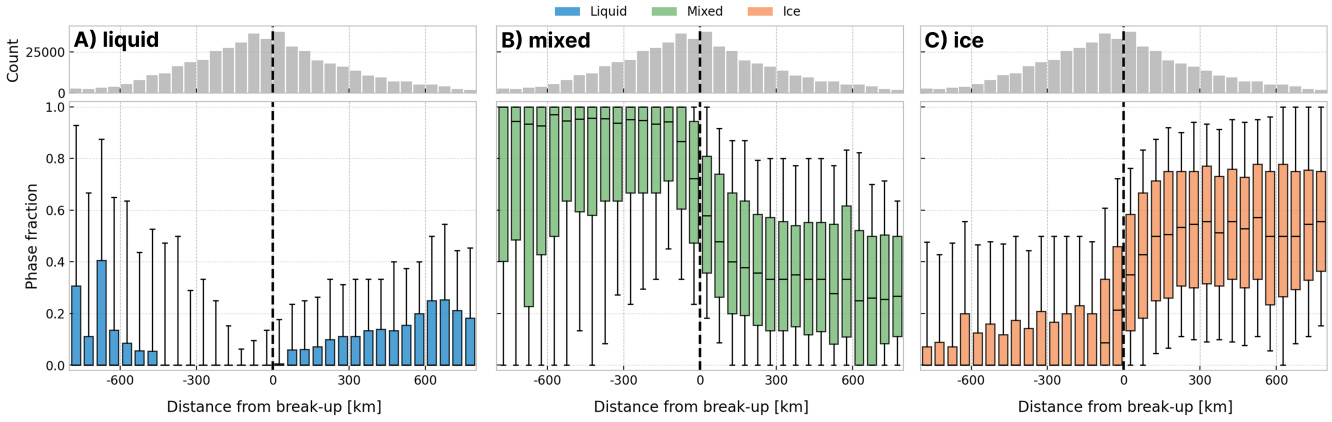


Figure E1. Liquid (A), mixed (B), and ice (C) phase fractions as a function of distance from break-up. Colored boxes represent the 25-75th percentiles, while the whiskers represent the 10-90th percentiles. Gray histograms represent the number of observations within each 50-km bin corresponding to the phase fractions.

Appendix F: Cloud top temperature, liquid and ice water paths

We also retrieve the ice water path from the combined CPR and CALIOP 2C-ICE product (Deng et al., 2010, 2013, 2015). To retrieve LWPs we used the combined Advanced Microwave Scanning Radiometer (AMSR) product: AMSR-E/AMSR2 Unified L2B Global Swath Surface Precipitation, Version 1 (Kummerow et al., 2020). Both AMSR instruments were part of the A-train constellation, allowing close to perfect temporal collocation with our wind transects. For the spatial collocation, we only use nadir pixels in order to provide the LWP at the same locations as the active remote sensing products.

A common problem when using microwave retrievals of LWP is the beam-filling error giving inaccurate in-cloud estimates for a non-uniform cloud field (Liu and Curry, 1993). As we are interested in the evolution of LWP as clouds break-up, it becomes especially important to account for this error. A common approach is to scale the LWP by the inverse of the cloud fraction (CF) (Greenwald et al., 1997):

$$\mathrm{LWP}_{\mathrm{scaled}} = \frac{\mathrm{LWP}}{\mathrm{CF}} \tag{F1}$$

To perform this scaling, we utilize the CLDMSK_L2_MODIS_Aqua product (VIIRS Atmosphere Science Team SSEC University Of Wisconsin-Madison, 2026) to calculate a cloud fraction, giving us the final scaled LWP.

Figure F1 shows the CTT, IWP, LWP, and the summed total water path (TWP) in panels A, B, C, and D, respectively. While the TWP quickly reaches relatively stable values as the clouds move off the ice edge, the development of IWP and LWP depend on the break-up distance from the ice edge. Clouds that travel farther than 600 km before breaking up tend to have higher LWPs and lower IWPs, whereas cases that break up closer to the ice edge exhibit lower LWPs and higher IWPs.

https://doi.org/10.5194/egusphere-2026-6553
Preprint. Discussion started: 9 November 2026
© Author(s) 2026. CC BY 4.0 License.

Because IWP retrievals are temperature dependent, we also examine CTT as shown in panel A. Regions of low IWP generally coincide with higher CTTs, suggesting a potential retrieval bias. Nevertheless, the AMSR LWP signal aligns with the IWP pattern, which increases our confidence that the observed partitioning reflects temperature-dependent ice production processes in the clouds, rather than retrieval artifacts.

For CAOs breaking up within 600 km of the ice edge, no clear dependence of CTT, IWP, or LWP on break-up distance is apparent, indicating that the role of CTT is not universal. This suggests that sufficiently high CTTs may favor alternative cloud evolutions influenced by processes beyond those discussed in H2 and H3.

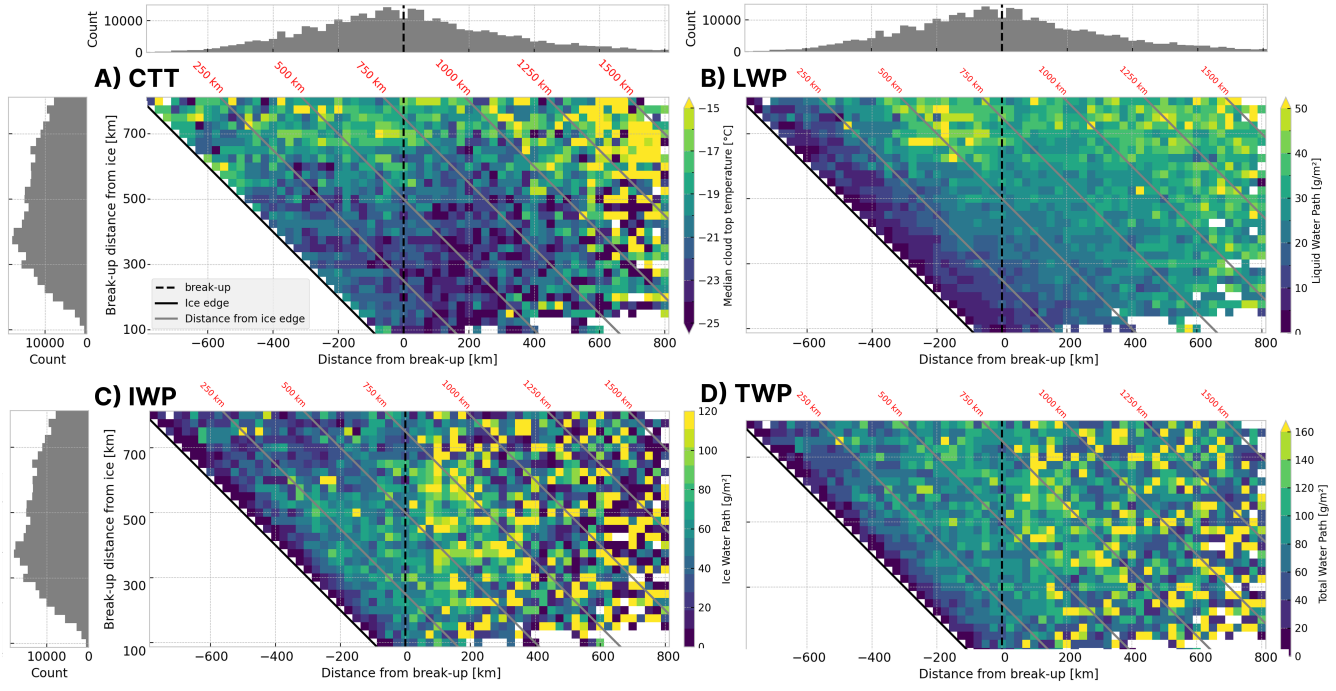


Figure F1. Cloud top temperatures (A), Liquid water path (B), ice water path (C), and total water path (D) as a function of distance from break-up and fetch at break-up.

Author contributions. FSVDL, ROD, and TC designed and conceptualized the study. FSVDL conducted the labeling, formal analysis and investigation, and developed the methodology with supervision from ROD, TC and TS. The manuscript was written by FSVDL with contributions from ROD, TC and TS.

Competing interests. The authors have declared that none of the authors have any competing interests.

https://doi.org/10.5194/egusphere-2026-6553
Preprint. Discussion started: 9 November 2026
© Author(s) 2026. CC BY 4.0 License.



Acknowledgements. This research was supported by the European Research Council through ERC Consolidator Grant STEP-CHANGE Grant 101045273 and ESA Earth Observation Envelope Programme (ESA-EOEP) contract No. 4000145240/24/NL/SC (CELLO). We acknowledge the use of imagery from the NASA Worldview application (https://worldview.earthdata.nasa.gov), part of the NASA Earth Science Data and Information System (ESDIS). We are also grateful to NRIS Sigma2 computing resources. Although generative AI was not directly involved in the writing of this manuscript, we acknowledge its use in suggesting language formulations.

https://doi.org/10.5194/egusphere-2026-6553
Preprint. Discussion started: 9 November 2026
© Author(s) 2026. CC BY 4.0 License.

References

Abel, S. J., Boutle, I. A., Waite, K., Fox, S., Brown, P. R. A., Cotton, R., Lloyd, G., Choularton, T. W., and Bower, K. N.: The Role of Precipitation in Controlling the Transition from Stratocumulus to Cumulus Clouds in a Northern Hemisphere Cold-Air Outbreak, Journal of the Atmospheric Sciences, 74, 2293–2314, https://doi.org/10.1175/JAS-D-16-0362.1, 2017.

Bergeron, T.: On the physics of clouds and precipitation, Proc. 5th Assembly U.G.G.I., Lisbon, Portugal, 1935, pp. 156–180, 1935.

Brümmer, B.: Roll and Cell Convection in Wintertime Arctic Cold-Air Outbreaks, Journal of the Atmospheric Sciences, 56, https://doi.org/10.1175/1520-0469(1999)056<2613:racciw>2.0.co;2, 1999.

Cao, Q., Hong, Y., Chen, S., Gourley, J. J., Zhang, J., and Kirstetter, P. E.: Snowfall Detectability of NASA's CloudSat : the First Cross-Investigation of Its 2c-Snow-Profile Product and National Multi-Sensor Mosaic QPE (NMQ) Snowfall Data, Progress In Electromagnetics Research, 148, 55–61, https://doi.org/10.2528/PIER14030405, 2014.

Carlsen, T. and David, R. O.: Spaceborne evidence that ice-nucleating particles influence high-latitude cloud phase, Geophysical Research Letters, 49, e2022GL098 041, https://doi.org/10.1029/2022GL098041, 2022.

Dahlke, S., Solbès, A., and Maturilli, M.: Cold air outbreaks in Fram Strait: Climatology, trends, and observations during an extreme season in 2020, Journal of Geophysical Research: Atmospheres, 127, e2021JD035 741, https://doi.org/10.1029/2021JD035741, 2022.

Deng, M., Mace, G. G., Wang, Z., and Okamoto, H.: Tropical Composition, Cloud and Climate Coupling Experiment validation for cirrus cloud profiling retrieval using CloudSat radar and CALIPSO lidar, Journal of Geophysical Research: Atmospheres, 115, https://doi.org/10.1029/2009JD013104, 2010.

Deng, M., Mace, G. G., Wang, Z., and Lawson, R. P.: Evaluation of Several A-Train Ice Cloud Retrieval Products with In Situ Measurements Collected during the SPARTICUS Campaign, Journal of Applied Meteorology and Climatology, 52, 1014–1030, https://doi.org/10.1175/JAMC-D-12-054.1, 2013.

Deng, M., Mace, G. G., Wang, Z., and Berry, E.: CloudSat 2C-ICE product update with a new Ze parameterization in lidar-only region, Journal of Geophysical Research: Atmospheres, 120, 12,198–12,208, https://doi.org/10.1002/2015JD023600, 2015.

DiGirolamo, N., Parkinson, C., Cavalieri, D., Gloersen, P., and Zwally, H.: Sea Ice Concentrations from Nimbus-7 SMMR and DMSP SSM/I-SSMIS Passive Microwave Data, Version 2, https://doi.org/10.5067/MPYG15WAA4WX, 2022.

Ephraim, S., Zuidema, P., Bansemer, A., Cai, L., Petters, M., Rosky, E., Snider, J. R., Wang, Z., Woods, S., Barry, K., Campos, T., Cruikshank, O., Eckhardt, S., Evangeliou, N., Foskinis, R., French, J. R., Geerts, B., Grasmick, C., Henning, S., Kumar, V., Massling, A., Mavis, C., McFarquhar, G. M., Nenes, A., Noer, G., Patnaude, R., Perkins, R., Sorensen, L. L., Skov, H., Tatro, T., Tornow, F., and Zhang, L.: A closed-to-open cell mixed-phase cloud transition observed over the Nordic Seas under high aerosol loading and strong surface fluxes, EGUsphere, pp. 1–47, https://doi.org/10.5194/egusphere-2026-2940, 2026.

Etling, D. and Brown, R. A.: Roll vortices in the planetary boundary layer: A review, Boundary-Layer Meteorology, 65, 215–248, https://doi.org/10.1007/BF00705527, 1993.

Findeisen, W.: Kolloid-meteorologische Vorgänge bei Niederschlagsbildung, Meteorologische Zeitschrift, 55, 121–133, 1938.

Fletcher, J. K., Mason, S., and Jakob, C.: A climatology of clouds in marine cold air outbreaks in both hemispheres, Journal of Climate, 29, 6677–6692, https://doi.org/10.1175/JCLI-D-15-0783.1, 2016.

Geerts, B., Giangrande, S. E., McFarquhar, G. M., Xue, L., Abel, S. J., Comstock, J. M., Crewell, S., DeMott, P. J., Ebell, K., Field, P., Hill, T. C. J., Hunzinger, A., Jensen, M. P., Johnson, K. L., Juliano, T. W., Kollias, P., Kosovic, B., Lackner, C., Luke, E., Lüpkes, C., Matthews, A. A., Neggers, R., Ovchinnikov, M., Powers, H., Shupe, M. D., Spengler, T., Swanson, B. E., Tjernström, M., Theisen, A. K., Wales,

https://doi.org/10.5194/egusphere-2026-6553
Preprint. Discussion started: 9 November 2026
© Author(s) 2026. CC BY 4.0 License.

N. A., Wang, Y., Wendisch, M., and Wu, P.: The COMBLE Campaign: A Study of Marine Boundary Layer Clouds in Arctic Cold-Air Outbreaks, Bulletin of the American Meteorological Society, 103, E1371–E1389, https://doi.org/10.1175/BAMS-D-21-0044.1, 2022.

Gelaro, R., McCarty, W., Suárez, M. J., Todling, R., Molod, A., Takacs, L., Randles, C. A., Darmenov, A., Bosilovich, M. G., Reichle, R., Wargan, K., Coy, L., Cullather, R., Draper, C., Akella, S., Buchard, V., Conaty, A., Silva, A. M. d., Gu, W., Kim, G.-K., Koster, R., Lucchesi, R., Merkova, D., Nielsen, J. E., Partyka, G., Pawson, S., Putman, W., Rienecker, M., Schubert, S. D., Sienkiewicz, M., and Zhao, B.: The Modern-Era Retrospective Analysis for Research and Applications, Version 2 (MERRA-2), Journal of Climate, 30, 5419 – 5454, https://doi.org/10.1175/JCLI-D-16-0758.1, place: Boston MA, USA, 2017.

Gjelsvik, A. B., David, R. O., Carlsen, T., Hellmuth, F., Hofer, S., McGraw, Z., Sodemann, H., and Storelvmo, T.: Using a region-specific ice-nucleating particle parameterization improves the representation of Arctic clouds in a global climate model, Atmospheric Chemistry and Physics, 25, 1617–1637, https://doi.org/10.5194/acp-25-1617-2025, 2025.

Global Modeling and Assimilation Office (GMAO): MERRA-2 tavg1_2d_slv_Nx: 2d,1-Hourly,Time-Averaged,Single-Level,Assimilation,Single-Level Diagnostics V5.12.4,, https://doi.org/10.5067/VJAFPLI1CSIV, 2015.

Goren, T., Kazil, J., Hoffmann, F., Yamaguchi, T., and Feingold, G.: Anthropogenic Air Pollution Delays Marine Stratocumulus Breakup to Open Cells, Geophysical Research Letters, 46, 14 135–14 144, https://doi.org/10.1029/2019GL085412, _eprint: https://agupubs.onlinelibrary.wiley.com/doi/pdf/10.1029/2019GL085412, 2019.

Greenwald, T. J., Christopher, S. A., and Chou, J.: Cloud liquid water path comparisons from passive microwave and solar reflectance satellite measurements: Assessment of sub-field-of-view cloud effects in microwave retrievals, Journal of Geophysical Research: Atmospheres, 102, 19 585–19 596, https://doi.org/10.1029/97JD01257, _eprint: https://agupubs.onlinelibrary.wiley.com/doi/pdf/10.1029/97JD01257, 1997.

Hallett, J. and Mossop, S. C.: Production of secondary ice particles during the riming process, Nature, 249, 26–28, https://doi.org/10.1038/249026a0, 1974.

Haynes, J. M., L'Ecuyer, T. S., Stephens, G. L., Miller, S. D., Mitrescu, C., Wood, N. B., and Tanelli, S.: Rainfall retrieval over the ocean with spaceborne W-band radar, Journal of Geophysical Research: Atmospheres, 114, https://doi.org/10.1029/2008JD009973, 2009.

Illingworth, A. J., Barker, H. W., Beljaars, A., Ceccaldi, M., Chepfer, H., Clerbaux, N., Cole, J., Delanoë, J., Domenech, C., Donovan, D. P., Fukuda, S., Hirakata, M., Hogan, R. J., Huenerbein, A., Kollias, P., Kubota, T., Nakajima, T., Nakajima, T. Y., Nishizawa, T., Ohno, Y., Okamoto, H., Oki, R., Sato, K., Satoh, M., Shephard, M. W., Velázquez-Blázquez, A., Wandinger, U., Wehr, T., and Zadelhoff, G.-J. v.: The EarthCARE Satellite: The Next Step Forward in Global Measurements of Clouds, Aerosols, Precipitation, and Radiation, Bulletin of the American Meteorological Society, 96, 1311–1332, https://doi.org/10.1175/BAMS-D-12-00227.1, 2015.

Karalis, M., Sotiropoulou, G., Abel, S. J., Bossioli, E., Georgakaki, P., Methymaki, G., Nenes, A., and Tombrou, M.: Effects of secondary ice processes on a stratocumulus to cumulus transition during a cold-air outbreak, Atmospheric Research, 277, 106 302, https://doi.org/10.1016/j.atmosres.2022.106302, 2022.

Klingebiel, M., Ehrlich, A., Gryschka, M., Risse, N., Maherndl, N., Schirmacher, I., Rosenburg, S., Hörnig, S., Moser, M., Jäkel, E., Schäfer, M., Deneke, H., Mech, M., Voigt, C., and Wendisch, M.: Airborne observations of cloud properties during their evolution from organized streets to isotropic cloud structures along an Arctic cold-air outbreak, Atmospheric Chemistry and Physics, 25, 9787–9801, https://doi.org/10.5194/acp-25-9787-2025, 2025.

Klingebiel, M., Luebke, A. E., Ehrlich, A., Mech, M., Sundermann, H., Deneke, H., Gryschka, M., Shupe, M. D., Zuidema, P., and Wendisch, M.: Observational Validation of Boundary-Layer Cloud Regimes in Arctic Cold Air Outbreaks, Geophysical Research Letters, 53, e2026GL124 831, https://doi.org/10.1029/2026GL124831, 2026.

https://doi.org/10.5194/egusphere-2026-6553
Preprint. Discussion started: 9 November 2026
© Author(s) 2026. CC BY 4.0 License.



Kolstad, E. W. and Bracegirdle, T. J.: Marine cold-air outbreaks in the future: an assessment of IPCC AR4 model results for the Northern Hemisphere, Climate dynamics, 30, 871–885, https://doi.org/10.1007/s00382-007-0331-0, 2008.

Korolev, A. and Leisner, T.: Review of experimental studies of secondary ice production, Atmospheric Chemistry and Physics, 20, 11 767–11 797, https://doi.org/10.5194/acp-20-11767-2020, 2020.

Kummerow, C., Ferraro, R., and Randel, D.: AMSR-E/AMSR2 Unified L2B Global Swath Surface Precipitation, Version 1, https://doi.org/10.5067/P5MCTDH7674A, 2020.

Larsgård, N. E., Carlsen, T., David, R. O., von der Lippe, F. S., Schwarzenboek, A., Sodemann, H., and Storelvmo, T.: The evolution of cloud microphysical properties during Cold Air Outbreaks – a composite approach to in situ measurements, EGUsphere, pp. 1–34, https://doi.org/10.5194/egusphere-2026-1650, 2026.

Liu, G. and Curry, J. A.: Determination of characteristic features of cloud liquid water from satellite microwave measurements, Journal of Geophysical Research: Atmospheres, 98, 5069–5092, https://doi.org/10.1029/92JD02888, 1993.

Lloyd, G., Choularton, T. W., Bower, K. N., Gallagher, M. W., Crosier, J., O'Shea, S., Abel, S. J., Fox, S., Cotton, R., and Boutle, I. A.: In situ measurements of cloud microphysical and aerosol properties during the break-up of stratocumulus cloud layers in cold air outbreaks over the North Atlantic, Atmospheric Chemistry and Physics, 18, 17 191–17 206, https://doi.org/10.5194/acp-18-17191-2018, 2018.

Mateling, M. E., Pettersen, C., Kulie, M. S., and L'Ecuyer, T. S.: Marine Cold-Air Outbreak Snowfall in the North Atlantic: A CloudSat Perspective, Journal of Geophysical Research: Atmospheres, 128, e2022JD038 053, https://doi.org/10.1029/2022JD038053, _eprint: https://agupubs.onlinelibrary.wiley.com/doi/pdf/10.1029/2022JD038053, 2023.

Mauritsen, T., Sedlar, J., Tjernström, M., Leck, C., Martin, M., Shupe, M., Sjogren, S., Sierau, B., Persson, P. O. G., Brooks, I. M., and Swietlicki, E.: An Arctic CCN-limited cloud-aerosol regime, Atmospheric Chemistry and Physics, 11, 165–173, https://doi.org/10.5194/acp-11-165-2011, 2011.

Mayer, J., Gasbarra, D., Hogan, R. J., Malina, E., Mason, S. L., and Piskala Gvozdikova, B.: EarthCARE reveals details on the role of rain in closed-to-open cell transitions, Atmospheric Chemistry and Physics, 26, 14 085–14 110, https://doi.org/10.5194/acp-26-14085-2026, 2026.

McCoy, I. L., Wood, R., and Fletcher, J. K.: Identifying meteorological controls on open and closed mesoscale cellular convection associated with marine cold air outbreaks, Journal of Geophysical Research: Atmospheres, 122, 11–678, https://doi.org/10.1002/2017JD027031, 2017.

MODIS Characterization Support Team (MCST): MODIS 1km Calibrated Radiances Product, https://doi.org/http://dx.doi.org/10.5067/MODIS/MOD021KM.061, 2017.

Monin, A. S. and Obukhov, A. M.: Basic laws of turbulent mixing in the ground layer of the atmosphere, Tr. Geofiz. Inst., Akad. Nauk SSSR, 24, 163–187, 1954.

Murray-Watson, R. J. and Gryspeerdt, E.: Air mass history linked to the development of Arctic mixed-phase clouds, Atmospheric Chemistry and Physics, 24, 11 115–11 132, https://doi.org/10.5194/acp-24-11115-2024, 2024.

Murray-Watson, R. J., Gryspeerdt, E., and Goren, T.: Investigating the development of clouds within marine cold-air outbreaks, Atmospheric Chemistry and Physics, 23, 9365–9383, https://doi.org/10.5194/acp-23-9365-2023, 2023.

Obukhov, A. M.: Turbulence in the atmosphere with inhomogeneous temperature, Tr. Inst. Teor. Geofiz., Akad. Nauk SSSR, 1, 95–115, 1946.

Papritz, L. and Spengler, T.: A Lagrangian climatology of wintertime cold air outbreaks in the Irminger and Nordic Seas and their role in shaping air–sea heat fluxes, Journal of Climate, 30, 2717–2737, https://doi.org/10.1175/JCLI-D-16-0605.1, 2017.

https://doi.org/10.5194/egusphere-2026-6553
Preprint. Discussion started: 9 November 2026
© Author(s) 2026. CC BY 4.0 License.

Papritz, L., Pfahl, S., Sodemann, H., and Wernli, H.: A Climatology of Cold Air Outbreaks and Their Impact on Air–Sea Heat Fluxes in the High-Latitude South Pacific, Journal of Climate, 28, 342 – 364, https://doi.org/10.1175/JCLI-D-14-00482.1, place: Boston MA, USA, 2015.

Pasquier, J. T., Henneberger, J., Ramelli, F., Lauber, A., David, R. O., Wieder, J., Carlsen, T., Gierens, R., Maturilli, M., and Lohmann, U.: Conditions favorable for secondary ice production in Arctic mixed-phase clouds, Atmospheric Chemistry and Physics, 22, 15 579–15 601, https://doi.org/10.5194/acp-22-15579-2022, 2022.

Renfrew, I. A. and Moore, G. W. K.: An Extreme Cold-Air Outbreak over the Labrador Sea: Roll Vortices and Air–Sea Interaction, Monthly Weather Review, 127, 2379–2394, https://doi.org/10.1175/1520-0493(1999)127<2379:AECAOO>2.0.CO;2, 1999.

Saggiorato, B., Nuijens, L., Siebesma, A. P., Roode, S. d., Sandu, I., and Papritz, L.: The Influence of Convective Momentum Transport and Vertical Wind Shear on the Evolution of a Cold Air Outbreak, Journal of Advances in Modeling Earth Systems, 12, e2019MS001 991, https://doi.org/10.1029/2019MS001991, 2020.

Sandu, I. and Stevens, B.: On the factors modulating the stratocumulus to cumulus transitions, Journal of the Atmospheric Sciences, 68, 1865–1881, https://doi.org/10.1175/2011JAS3614.1, 2011.

Sassen, K., Wang, Z., and Liu, D.: Global distribution of cirrus clouds from CloudSat/Cloud-Aerosol Lidar and Infrared Pathfinder Satellite Observations (CALIPSO) measurements, Journal of Geophysical Research: Atmospheres, 113, https://doi.org/10.1029/2008JD009972, 2008.

Stephens, G., Winker, D., Pelon, J., Trepte, C., Vane, D., Yuhas, C., L'Ecuyer, T., and Lebsock, M.: CloudSat and CALIPSO within the A-Train: Ten Years of Actively Observing the Earth System, Bulletin of the American Meteorological Society, 99, 569–581, https://doi.org/10.1175/BAMS-D-16-0324.1, 2018.

Stephens, G. L., Vane, D. G., Boain, R. J., Mace, G. G., Sassen, K., Wang, Z., Illingworth, A. J., O'connor, E. J., Rossow, W. B., Durden, S. L., Miller, S. D., Austin, R. T., Benedetti, A., and Mitrescu, C.: THE CLOUDSAT MISSION AND THE A-TRAIN: A New Dimension of Space-Based Observations of Clouds and Precipitation, Bulletin of the American Meteorological Society, 83, 1771–1790, https://doi.org/10.1175/BAMS-83-12-1771, 2002.

Tornow, F., Ackerman, A. S., and Fridlind, A. M.: Preconditioning of overcast-to-broken cloud transitions by riming in marine cold air outbreaks, Atmospheric Chemistry and Physics, 21, 12 049–12 067, https://doi.org/10.5194/acp-21-12049-2021, 2021.

Tornow, F., Ackerman, A. S., Fridlind, A. M., Tselioudis, G., Cairns, B., Painemal, D., and Elsaesser, G.: On the Impact of a Dry Intrusion Driving Cloud-Regime Transitions in a Midlatitude Cold-Air Outbreak, Journal of the Atmospheric Sciences, 80, 2881–2896, https://doi.org/10.1175/JAS-D-23-0040.1, 2023.

Torri, G., Kuang, Z., and Tian, Y.: Mechanisms for convection triggering by cold pools, Geophysical Research Letters, 42, 1943–1950, https://doi.org/10.1002/2015GL063227, 2015.

VIIRS Atmosphere Science Team SSEC University Of Wisconsin-Madison: MODIS/Aqua Cloud Mask and Spectral Test Results 5-Min L2 Swath 1km, https://doi.org/10.5067/MODIS/CLDMSK_L2_MODIS_AQUA.002, 2026.

von der Lippe, F. S., Carlsen, T., Storelvmo, T., and David, R. O.: Shortening of the Arctic cold air outbreak season detected by a phenomenological machine learning approach, Atmospheric Chemistry and Physics, 26, 1565–1585, https://doi.org/10.5194/acp-26-1565-2026, 2026.

Wegener, A.: Thermodynamik der atmosphäre, J. A. Barth, Leipzig, 1911.

Wehr, T., Kubota, T., Tzeremes, G., Wallace, K., Nakatsuka, H., Ohno, Y., Koopman, R., Rusli, S., Kikuchi, M., Eisinger, M., Tanaka, T., Taga, M., Deghaye, P., Tomita, E., and Bernaerts, D.: The EarthCARE mission – science and system overview, Atmospheric Measurement Techniques, 16, 3581–3608, https://doi.org/10.5194/amt-16-3581-2023, 2023.

https://doi.org/10.5194/egusphere-2026-6553
Preprint. Discussion started: 9 November 2026
© Author(s) 2026. CC BY 4.0 License.



Winker, D. M., Vaughan, M. A., Omar, A., Hu, Y., Powell, K. A., Liu, Z., Hunt, W. H., and Young, S. A.: Overview of the CALIPSO Mission and CALIOP Data Processing Algorithms, Journal of Atmospheric and Oceanic Technology, 26, 2310–2323, https://doi.org/10.1175/2009JTECHA1281.1, 2009.

Wood, N. B. and L'Ecuyer, T. S.: Level 2C Snow Profile Process Description and Interface Control Document, Product Version P1 R05. NASA JPL CloudSat project document revision 0., 26 pp. Available from https://www.cloudsat.cira.colostate.edu/cloudsat-static/info/dl/2c-snow-profile/2C-SNOW-PROFILE_PDICD.P1_R05.rev0_.pdf, 2018.

Wood, N. B., L'Ecuyer, T. S., Bliven, F. L., and Stephens, G. L.: Characterization of video disdrometer uncertainties and impacts on estimates of snowfall rate and radar reflectivity, Atmospheric Measurement Techniques, 6, 3635–3648, https://doi.org/10.5194/amt-6-3635-2013, 2013.

Wood, N. B., L'Ecuyer, T. S., Heymsfield, A. J., Stephens, G. L., Hudak, D. R., and Rodriguez, P.: Estimating snow microphysical properties using collocated multisensor observations, Journal of Geophysical Research: Atmospheres, 119, 8941–8961, https://doi.org/10.1002/2013JD021303, 2014.

Wood, R. and Bretherton, C. S.: On the Relationship between Stratiform Low Cloud Cover and Lower-Tropospheric Stability, Journal of Climate, 19, 6425 – 6432, https://doi.org/10.1175/JCLI3988.1, place: Boston MA, USA, 2006.

Yamaguchi, T., Feingold, G., and Kazil, J.: Stratocumulus to cumulus transition by drizzle, Journal of Advances in Modeling Earth Systems, 9, 2333–2349, https://doi.org/10.1002/2017MS001104, 2017.